Materials and Design 111 (2016) 362–368

Contents lists available at ScienceDirect

Materials and Design

journal homepage: www.elsevier.com/locate/matdes

# Elastomer-metal laminate armor

R.M. Gamache [a], C.B. Giller [b,c], G. Montella [b], D. Fragiadakis [d], C.M. Roland [d,*]

[a] Naval Postgraduate School, Monterey, CA, United States
[b] American Society for Engineering Education postdoctoral fellow, United States
[c] MITRE, McLean, VA, United States
[d] Naval Research Laboratory, Chemistry Division, Code 6100, WA 20375-5342, United States

## HIGHLIGHTS

- Polymer-aluminum laminates on the strike-face of steel plates enhance ballistic performance.
- With judicious selection of substrate and laminate, a broad range of performance and weight combinations can be obtained.
- There is both a reduction in magnitude of the substrate deformation and spatial dispersion of the impact.
- The main function of the metallic layers is to stiffen the polymer without affecting the latter's viscoelasticity response.

## GRAPHICAL ABSTRACT

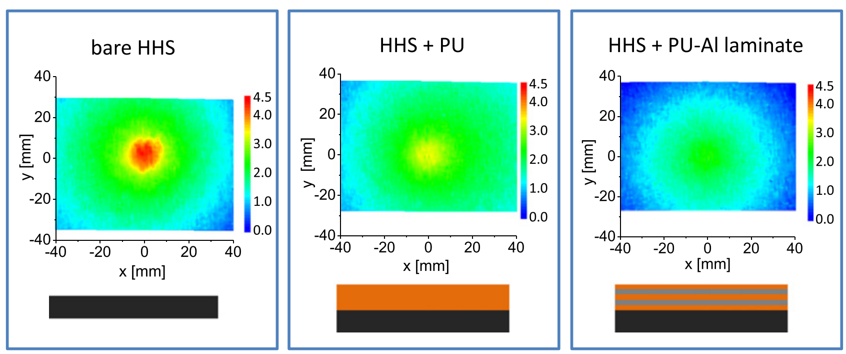


## ARTICLE INFO

*Article history:*
Received 28 June 2016
Received in revised form 23 August 2016
Accepted 24 August 2016
Available online 26 August 2016

*Keywords:*
Laminate
Wave transmission
Ballistics

## ABSTRACT

A study was carried out of pressure wave transmission and the ballistic penetration of steel substrates incorporating a front-face laminate, the latter consisting of alternating layers of thin metal and a soft polymer; the latter undergoes a viscoelastic phase transition on impact. The ballistic properties of laminate/steel structures are substantially better than conventional military armor. This enhanced performance has three origins: large energy absorption by the viscoelastic polymer, a significant strain-hardening of the material, and lateral spreading of the impact force. These mechanisms, active only at high strain rates, depend on the chemical structure of the polymer but not on the particular metal used in the laminate.

Published by Elsevier Ltd.

## 1. Introduction

Reflecting the need to meet the disparate requirements of military armor (e.g., performance, size, and weight), the use of layered and laminated structures is not uncommon. The impact resistance of multiple thin metallic plates has been found to be better [1,2] or worse [3,4] than that of fewer thick plates, the relative performance depending on the materials, their arrangement, and the shape of the projectile ogive [5,6,7]. Polymers are eight times less dense than steel and thus an obvious route to lighter structures. A prominent example of their application is transparent armor, a laminate of inorganic glass and polymer layers that affords rigidity, toughness, and resistance to crack propagation [8,9,10,11]. Fiber composites are often layered with harder materials such as steel to yield better performance for a given weight [12]. A key to obtaining good ballistic properties with laminates is to maximize any available energy absorption mechanisms [13,14,15,16]; these can include friction between the projectile and the armor material, deformation (e.g., shearing and back side deflection) of the components, and layer delamination. For composites, especially fiber-reinforced

* Corresponding author.
*E-mail address:* roland@nrl.navy.mil (C.M. Roland).

http://dx.doi.org/10.1016/j.matdes.2016.08.072
0264-1275/Published by Elsevier Ltd.

materials, the primary modes of energy loss are fiber strain and breakage, and debonding from the matrix [17,18,19,20]. Cuniff [21] proposed a performance metric for fiber composites that indicates the ballistic limit (minimum projectile velocity for complete penetration) depends sublinearly on the modulus, strength, and failure strain of the fibers. For laminate armor, shear deformation promoted by the layering can have a substantial influence on the impact response [22], as can interaction between the layers [12]. The presence of a front-face polymer structure can even alter the failure mode of the underlying steel substrate [23,24]. Shear-plugging and spallation are the usual failure mechanisms for hard steel subjected to the impact by a blunt projectile. In addition to attenuating the stress waves, front layers broaden the impact area with consequent reduction in impact pressure [25]. These effects reduce the tendency of the steel substrate to form a shear plug. Multiple layers also afford a method of mitigating ballistic impact through management of the shock wave (e.g., deflection and spreading) [26,27,28]. For these reasons, the stacking sequence can exert a significant influence on performance [29,30,31,32].

Herein results are presented for armor incorporating alternating thin layers of metal and a rubbery polymer, with this laminate structure placed on the front side of a steel substrate. The work evolved from earlier studies on bilayers consisting of steel with a thin elastomer coating [33,34,35,36,37], the unique feature therein the large contribution of viscoelasticity to the absorption of impact energy. The particular polymers employed have segmental dynamics occurring on the time scale of the ballistic impact (ca. $10^{-5}$ s), so that the impact induces a rubber-to-glass viscoelastic phase change [38]. This phase transition corresponds to the mechanical regime in which polymers are most energy dissipative. The mechanism is only operative in polymers having a glass transition temperature close to, but below, the test temperature, whereby local motion of the chain segments coincides with the ballistic impact. One curious feature of the polymer-coated steel is the dependence of penetration velocity on coating thickness [33,34]. There are two regimes: a steep linear increase up through thicknesses in the range 1–3 mm, followed by a second linear range with a much weaker dependence. This suggests employing multiple substrate-coating assemblies to take better advantage of the coating; that is, use a laminate design. In addition, by incorporating the polymers in multiple layers, the mechanical stiffness of the coating is increased, which affects transmission of the pressure wave and promotes its spatial and temporal dispersion. Different laminate designs were tested, and the results compared to the ballistic performance of Rolled Homogeneous Armor (RHA; MIL-DTL-12,560), a traditional material which served as the primary military armor through the Second World War.

## 2. Experimental

The polymer was a polyurea (PU) obtained by reaction of 1 part isocyanate (Isonate 143L from Dow Chemical) with 4 parts polydiamine (Air Product's Versalink P1000, having a molecular weight of 1 kg/mol). The elastomeric material had a calorimetric glass transition temperature equal to −60 °C. The application of the polymer for ballistic armor is described in several publications [39,40,41,42]. The metal for the laminate was either aluminum (2024-T3 alloy) or titanium (grade 2). Plates of High Hard Steel (HHS, Mil-A-46100E; Brinell hardness ~500) or Ultra High Hard Steel (UHHS; Brinell hardness ~600) served as the substrate.

Very generally, the performance of multi-layer armor is affected by the shape of the projectile, with blunt ogives being more easily defeated [1,43]. The impact-induced phase transition, which is a primary source of energy dissipation for the designs herein, relies on rapid compression of the polymer coating by the projectile. For this reason the present experiments were limited to flat-faced projectiles; specifically, 0.50 caliber fragment-simulating projectiles (fsp; Mil-DTL-46593B). Their Brinell hardness is $285 \pm 1$; that is, the fsp are softer than either steel substrate, and become highly compressed and highly distorted by passage through the target. The details of the ballistic testing can be found elsewhere [44]. Briefly, projectile velocities, determined using tandem chronographs, were varied over the range 300–1500 m/s, according to the quantity of gun powder (2 to 15 g of IMR 4895). The measure of ballistic performance was V-50 (Mil-Std-662F), the projectile velocity for which there is a 50% probability of complete penetration of the target, calculated as the average of the lowest and highest velocities for complete penetration and partial penetration, respectively. The former requires perforation, either by the projectile itself or from spall, of a 0.5 mm aluminum (2024 T3) witness plate located 15 cm behind the target. Some ballistic results herein are reported after normalization by the V-50 of RHA; (Brinell ~380). A metric that include the armor weight in assessing performance is mass efficiency, defined as the inverse fractional weight reduction achieved relative to the use of RHA having the same V-50; for the latter is obtained from interpolation of data in MIL-DTL-12560J, Table A-IV.

Digital image correlation (DIC) experiments [45] were carried out at the Army Research Lab to measure deformations during ballistic testing. Two high-speed video cameras (150,000 frames/s) were used to stereoscopically track the displacement of a fiducial pattern on the backside of the target; spatial resolution was 2 mm. The projectile was the 0.50 cal fsp at a speed on impact equal to $610 \pm 30$, which is 84% of the V-50 of the 7.3 mm HHS substrate. This speed corresponds to a strain rate for the coating of ca. $10^5$ $s^{-1}$. Data were acquired every 6 μs.

High strain rate compression tests of the laminates at room temperature were carried out using a split Hopkinson pressure bar apparatus (SPHB) [46,47]. All bars were 6061-T6 aluminum with a diameter of 15.9 mm and a specific acoustic impedance measured to be to $16.9 \pm 1$ MRayl at 1 MHz. The incident and transmission bars had a common length of 1830 mm; the striker bar was 304 mm long. An annealed copper disk was employed to shape the incident pulse and allow a more gradual rise in the applied stress. Two sample configurations were tested using the SHPB: homogeneous polyurea and a laminate made of four alternating layers of the PU and aluminum 1100-O adhered with cyanoacrylate. The areal densities (weight per unit strike-face area) were the same, with the sample geometry chosen to have a height to diameter ratio <0.5 to minimize inertial effects and friction between the sample and bar. Silicone lubricant was applied to the faces to ensure slippage. The axial strains in the bars were monitored at two locations: 900 mm from the bar/specimen interface on the incident bar and 300 mm from the bar/specimen interface on the transmitted bar.

## 3. Results

### 3.1. Ballistic testing

In Fig. 1 are ballistic results for HHS with a front-surface laminate, the latter having different numbers of component layers, with the layer thickness varied to maintain a constant areal density (=55.3 kg/m$^2$). Optimal performance was obtained for 8 bilayers of 0.4 mm aluminum layered with 0.2 mm PU; however, variation in ballistic performance for the different constructions was only ca. 10%. Substitution of Ti for the Al slightly reduced the V-50 (by <4%), even though the former is almost 40% higher in ultimate strength at equal weight. This minor effect on performance of the inherent strength of the layer materials is illustrated by comparing ballistic performance of identical laminates, except that the metallic layers were either 1100-O or 2024-T3 type aluminum (Table 1). The latter has fivefold higher tensile strength and an order of magnitude higher yield stress; however, it yields only a 3% increase in V-50. These results clearly indicate that it is not the strength of the laminate per se that governs the enhanced resistance to ballistic penetration.

Other details of the laminate configuration similarly have only a modest effect on performance. For example, introducing a gradient in laminate thickness increased V-50 by 2.4% at constant weight (Table

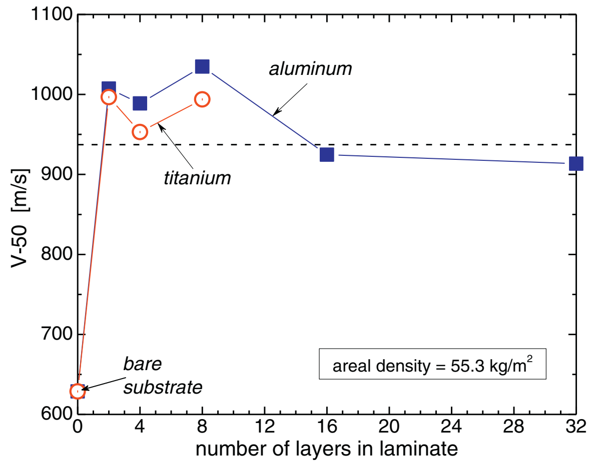


**Fig. 1.** Ballistic data for laminate constructions on 5.3 mm HHS substrates at constant weight per unit area. There is a minimal difference between aluminum and titanium layers. The dashed line indicates the performance of a polyurea-coated HHS bilayer (no laminate) having the same areal density. The error bars are not greater than the symbol size.

2). Perforation of the laminates increases V-50 by similar amounts, but with a small (ca. 4%) weight reduction (Table 3).

The data in Fig. 1 and Tables 1–3 show that changes in the laminate/steel construction has a surprisingly small effect (<5%) on performance. Of course, using more material (e.g., more or thicker layers) enhances performance, as shown in Fig. 2. The relevant question is how does the V-50 of the laminate compare to that achieved using only steel. To assess this, the ballistic results in Fig. 2 are also plotted as a function of mass efficiency; as can be seen, a front-surface laminate enables weight reductions of as much as a factor of two at equal V-50.

In Fig. 3 are collected ballistic data for a variety of laminates having different constructions; the substrate is HHS or UHHS. Two observations: (i) at constant weight, increases in V-50 of as much as 50% over the bare steel substrate are obtained, corresponding to mass efficiencies as high as 2. (ii) There is no systematic effect of substituting UHHS for HHS as the substrate. This is in contrast to steel having a homogeneous PU coating. For such simple bilayers, the V-50 increment due to the elastomer coating increases with increasing substrate hardness [25].

### 3.2. Digital image correlation

To investigate the mechanism underlying the effect of the laminate on the penetration resistance of steel substrates, the in-plane and out-of-plane displacements were measured on HHS (1.6 mm thick) bare, with a PU coating, and with a front-surface laminate consisting of 3 alternating layers of 2024-T3 Al (0.4 mm thick) and PU (0.8 mm thick). Results are shown in Fig. 4. The in-plain strain peaks around 17% for the uncoated HHS. This is reduced to <9% when the laminate is present, with intermediate behavior for the PU coating. There are comparable reductions in the deformation along the projectile direction, as can be seen. The maximum out-of-plane velocity, observed around 15–20 μs, was reduced from 170 to 130 m/s for the composite structure. These are significant reductions, which translate at higher projectile velocities to increased penetration resistance.

**Table 1**
Effect of laminate metal on ballistic performance.

| Substrate | No. of bilayers[a] | Al type | Areal density | V-50 (m/s) | Mass efficiency[b] |
|---|---|---|---|---|---|
| 7.3 mm HHS | 4 | 1100-O | 70.9 kg/m$^2$ | 1177 ± 14 | 1.54 ± 0.02 |
| | | 2024-T3 | | 1216 ± 10 | 1.59 ± 0.01 |

[a] Each 0.8 mm PU and 0.8 mm Al.
[b] Relative to RHA.

**Table 2**
Effect of gradient in laminate thickness on ballistic performance.

| Substrate | No. of bilayers[a] | Al type | Areal density (kg/m$^2$) | Laminate gradient[b] | V-50 (m/s) | Mass efficiency |
|---|---|---|---|---|---|---|
| 7.3 mm HHS | 4 | 1100-O | 70.9 | None | 1177 | 1.68 |
| | | 1100-O | | Increasing | 1206 | 1.58 |
| | | 1100-O | | Decreasing | 1181 | 1.55 |
| 5.1 mm HHS | | 2024-T3 | 53.8 | None | 979 | 1.68 |
| | | 2024-T3 | | Increasing | 994 | 1.70 |

[a] Each 0.8 mm PU and 0.8 mm Al.
[b] From front surface towards substrate.

The other effect of the PU coating or laminate is to spread the impact force laterally, which reduces the pressure. This results in a larger back-face deformation area and larger penetration hole than observed for bare steel substrates [25]. The transverse broadening is illustrated in Fig. 5, showing the in-plane strain as a function of distance from the point of impact. The strain is lowest when the laminate is present, and it decays over the greatest distance from the impact point. This reduces the impact pressure, and the additional work to deform the larger area enhances ballistic performance.

### 3.3. Split Hopkinson pressure bar tests

From the SHPB measurements the compressive stress-strain curves can be obtained [48]. These are shown in Fig. 6 for the homogenous PU coating and the laminate, both at a nominal strain rate of 2000 s$^{-1}$. This rate is at least two orders of magnitude slower than necessary to induce a transition to the glassy state [36], so although the polymer exhibits a high degree of viscoelasticity, it remains a rubber. As can be seen, the laminate is roughly 1.5 times stiffer than the polyurea, corresponding to a proportionally greater strain energy.

Analysis of the stress waves enables an assessment of any role of impedance mismatching in the laminate. Fig. 7 shows the incident, reflected, and transmitted waves measured for the polyurea and the laminate. As can be seen, there is negligible difference between the two samples for either the length or amplitude of the transmitted pulses. The maximum amplitude of the stress wave, $P_t$, and the impulse, $I_t$, transmitted through the samples, can be calculated by assuming an elastic structure behind the transmission bar having the corresponding values of $P_o$ and $I_o$. For the three dimensional case, the impedance of the material, Z, is given by the product of the density, ρ, the acoustic velocity, v, and the area, A. Due to geometry restrictions when testing nearly incompressible, soft materials, the diameter of the sample cannot exceed the diameter of the bars. Herein the samples have a smaller diameter than the bar, and thus a different area. As a pressure wave propagates through the sample, at each boundary the pressure wave experiences an impedance mismatch, causing a fraction, R, of the energy to be reflected and a fraction, T, to be transmitted to the next layer [49].

$$R = \frac{Z_{al} - Z_s}{Z_{al} + Z_s}, \quad T = \frac{2Z_{al}}{Z_{al} + Z_s}$$

where the subscripts refer to the sample and the aluminum impedances.

**Table 3**
Effect of perforations in laminate Al on ballistic performance.

| Substrate | No. of bilayers[a] | Void volume of metal | Areal density (kg/m$^2$) | V-50 (m/s) | Mass efficiency |
|---|---|---|---|---|---|
| 5.1 mm HHS | 4 | 0 | 53.8 | 979 | 1.54 |
| | | 23% | 52.3 | 997 | 1.75 |
| | | 40% | 51.8 | 1002 | 1.79 |

[a] Each 0.8 mm PU and 0.8 mm Al.

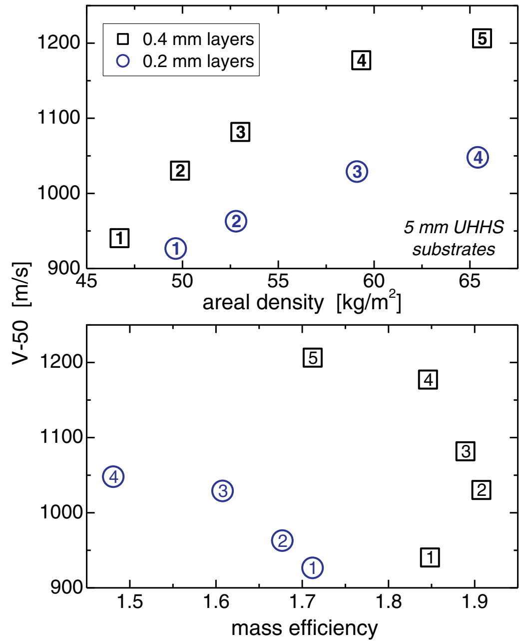


**Fig. 2.** Ballistic results for laminates with equal polyurea and Al thicknesses (indicated). Number of layers: (squares) 1–9, 2–13, 3–17, 4–25, 5–22; (circles) 1–25, 2–33, 3–49, 4–65. Compared at equal weight, thicker layers provide better performance and thus higher mass efficiencies.

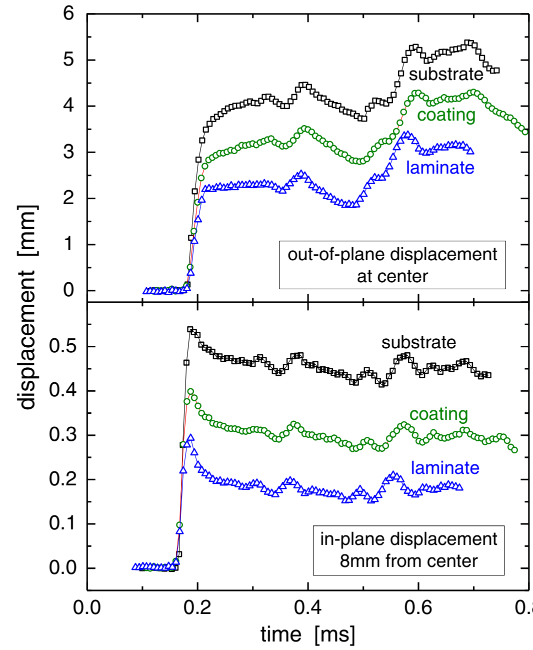


**Fig. 4.** Digital image correlation results for HHS substrate bare (squares), and with front-side PU coating (circles) or 3-layer Al/PU laminate (triangles). The deformation behavior is qualitatively the same, but substantial less for the laminate.

The peak transmitted and incident pressures, $P_t$ and $P_0$, are taken to be the maximum value of the respective longitudinal stresses. The impulse $I_t$ and $I_0$ are determined by integrating the longitudinal stress over the respective pulse. These results are listed In Table 4. Also tabulated are the transmitted, reflected, and absorbed energies. It is seen that the structure of the target exerts a modest effect. At least at the SHPB strain rates, which are two orders of magnitude lower than ballistic strain rates, the contribution of the laminate structure appears to be limited to stiffening of the polymer layer due to the metallic layers.

However, this stiffening does not affect the viscoelastic response of the polymer, in particular its capacity to dissipate energy; that is, hardening of the polymeric coating per se does not enhance ballistic performance. This is illustrated in Fig. 8, which compares the V-50 of HHS coated with PU to that for various polyethylene coatings. (The Young's moduli values are for low strain rate, but representative of the relative hardness of these materials.) The polyurea is superior because of its substantial energy dissipation and significant strain-hardening. The polyethylenes are semi-crystalline, which increases the Young's modulus but reduces their mechanical hysteresis. Thus, while hardness may increase resistance to penetration, this putative gain is negated by the decrement in energy dissipation.

### 3.4. Modeling

It is surprising that the waves transmitted by a homogeneous polymer layer and the laminate are essentially the same; that is, there is no indication of temporal or spatial dispersion arising from the laminate structure. For this reason the SHPB data were confirmed by numerical simulation. A finite element model was constructed using the commercial code Abaqus/Explicit (Version 6.10) with eight-node, reduced integration and hourglass control elements C3D8R [50]. The experiments

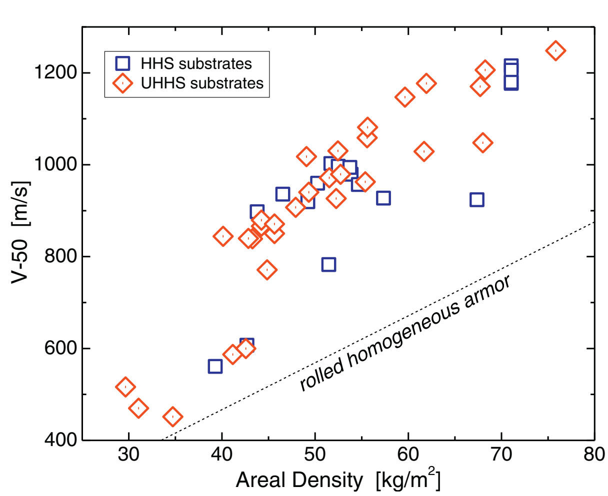


**Fig. 3.** Collected ballistic data for various laminate constructions on HHS or UHHS substrates; mass efficiencies range from 1.1 to 2.0. The dashed line represents V-50 for bare RHA.

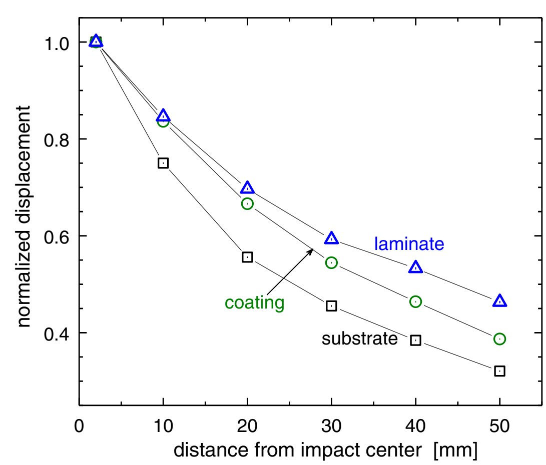


**Fig. 5.** Digital image correlation measurements of the maximum lateral displacement on backside of bare HHS (filled squares), and HSS with a polyurea (circles) or laminate (triangles) on front surface, plotted versus the distance from the projectile impact. Note the displacements are normalized by the maximum value to illustrate the more gradual decay ("force spreading") when a coating or laminate is present.

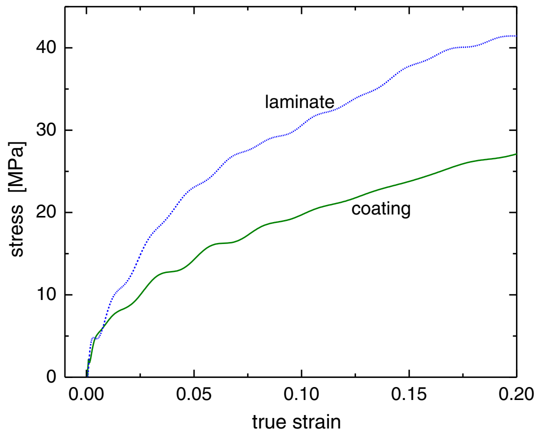


**Fig. 6.** Stress-strain behavior of the polyurea and the laminate measured in compression. Mean strain rate 2000 $s^{-1}$.

were simulated by using pressure as an external load and following its time evolution during a test. The aluminum components of the instrument are linearly elastic, with the density, Young's modulus E, and Poisson's ratio $\nu$ listed in Table 5.

Polyurea is modeled as a non-linear, viscoelastic material by employing a constitutive equation with separable strain-dependent and dimensionless time-dependent functions

$$\sigma(\varepsilon,t)=\sigma_0(\varepsilon)g(t)$$

For the strain dependence the Ogden equation [51] was used

$$W=\frac{2\mu}{\alpha}\left(\lambda_1^\alpha+\lambda_2^\alpha+\lambda_3^\alpha-3\right)$$

in which $\lambda_i$, $i=1,2,3$ are the principal stretches. The parameters $\mu$ and $\alpha$ are determined from fits to the experimental data of Sarva et al. [52] for this same PU deformed at very low strain rate (0.0016 $s^{-1}$). The time-dependent function is represented as a Prony series

$$g(t)=g_\infty+\sum_{i=1}^{3}g_i\exp\left(\frac{-t}{\tau_i}\right)$$

where $\tau_i$ are time constants and $g_\infty$ and $g_i$ are dimensionless constants. These parameters (Table 6) are quantified from the high strain rate measurements herein on the PU, following an approach suggested by Taylor et al. [53]. The time step in the analysis was chosen to be 10% of the period associated with the highest frequency seen in the experimental signal; the mesh size was 10% of the shortest wavelength. The Courant–Friedrichs–Lewy condition was met by setting the Courant number to 0.1.

Fig. 9 compares the experimental data to the calculated stresses. The agreement is qualitatively satisfactory, although it is not quantitative.

**Table 4**
Performance assessment of the different targets.

| Target | $P_t/P_0$ [%] | $I_t/I_0$ [%] | Transmitted energy [%] | Reflected energy [%] | Strain energy [%] |
|---|---|---|---|---|---|
| Polyurea | 13 | 37 | 2 | 63 | 30 |
| Laminate | 58 | 50 | 5 | 50 | 40 |

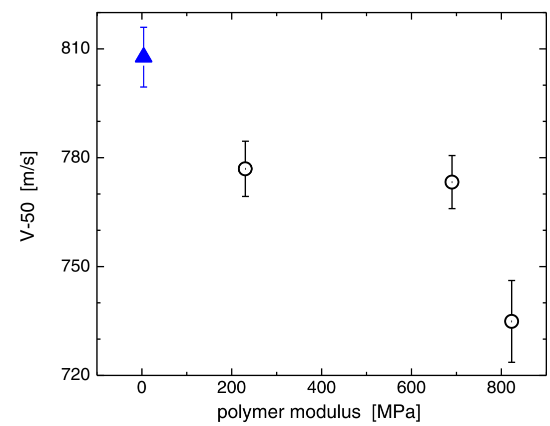


**Fig. 8.** Penetration velocity for 6.4 mm thick HHS with a 2.5 mm coating of polyurea (triangle) or polyethylene (circles); the latter have different Young's moduli due to varying degrees of crystallinity.

**Table 5**
Material properties for bars.

| Aluminum 6061-T6 | ρ [kg m$^{-3}$] | E [MPa] | $\nu$ |
|---|---|---|---|
| | 2708 | $6.98\times10^4$ | 0.33 |

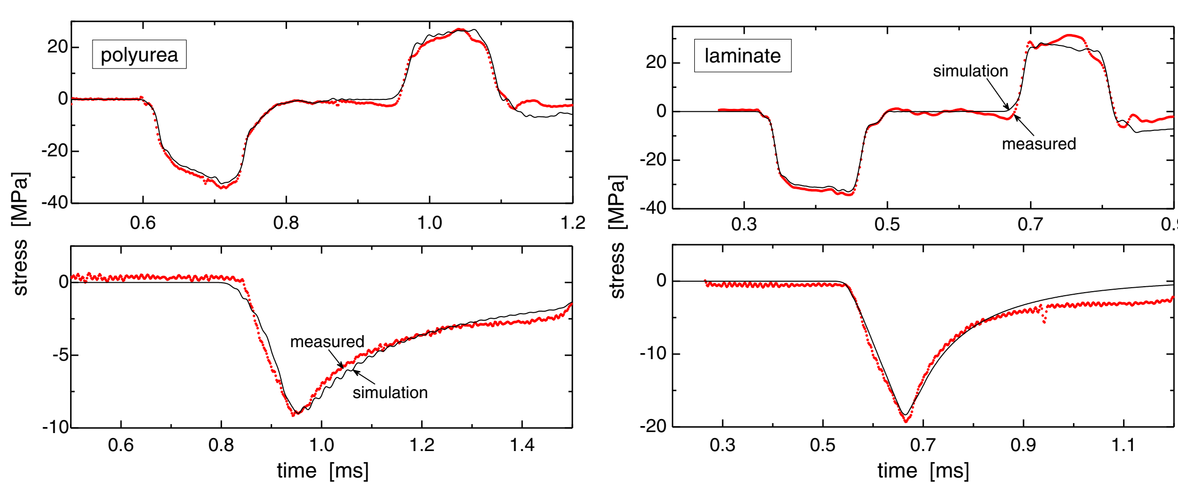


**Fig. 7.** Measured and computed pressure pulses for (left) polyurea and (right) laminate having two bilayers of the polymer and aluminum. Upper panels are the incident and reflected stress waves; lower are the transmitted wave.

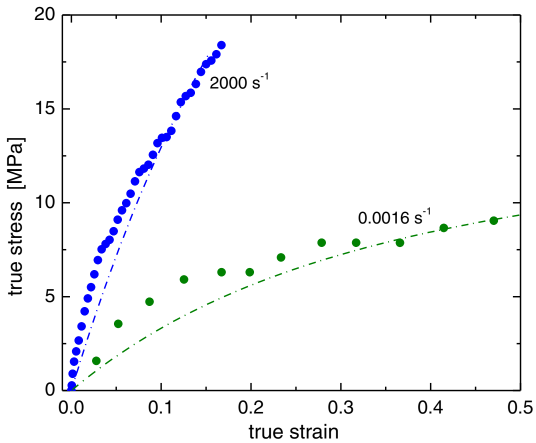


**Fig. 9.** Experimental stress-strain data for polyurea at different strain rates (symbols), along with from curves calculated using the Ogden/Prony series model (lines). The lower strain rate data is from ref. [52].

The deviations arise due to a number of factors, including non-constant strain rate during the Hopkinson bar measurements, the known limitations of the Ogden model, and the approximation entailed in assuming decoupling of strain and rate effects [51]. Nevertheless, the modeling confirms that the SHPB measurements capture the key aspects of wave transmission through the polymer coating and the laminate, with the caveat that extension of these results to ballistic performance is limited due to the difference in strain rates.

## 4. Summary

Soft elastomers that undergo a viscoelastic phase transition under impact loading have been found to improve significantly the ballistic properties of steel when applied as a front surface coating. The results herein show that polymer-metal laminates similarly confer enhanced ballistic performance. Interestingly the details of the laminate construction, including the number of layers and the nature of the metal component, have a very small effect of the properties. Consistent with these results, DIC and Hopkinson bar measurements indicate the principal role of the laminate construction is to stiffen the coating. The key attribute of a laminate structure is that this stiffening comes without any direct effect on the polymer. Increasing the coating hardness by modifying the material, via crosslinking [33], fillers [34], or partial crystallinity (Fig. 8), is less effective because it reduces the energy dissipative capacity of the material. The laminate approach does not interfere with the impact-induced glass transition mechanism central to the ballistic properties of the polyurea. Note that the hardness of the underlying substrate directly affects the contribution of the coating, although this coupling of the substrate and coating remains to be fully understood [25].

**Table 6**
Material properties for polyurea.

| Ogden parameters | | | |
|---|---|---|---|
| μ [MPa] | | | A |
| 13.417 | | | −2.25 |
| Prony series constants | | | |
| $\tau_i$ [s] | 0.001 | 1 | 1000 |
| $g_i$ | 0.61002 | 0.06250 | 0.00265 |

## Acknowledgements

This work was supported by the Office of Naval Research, substantially by ONR Code 332 (R.G. Barsoum). GM and CBG expressed their appreciation for American Society of Engineering Education/Naval Research Laboratory postdoctoral fellowships. We thank J. Lee and J. Polesne of the Army Research Lab for carrying out the DIC measurements and D. Calvo of NRL for determining the wave speed in the aluminum bars.

## References

[1] X. Teng, S. Dey, T. Børvik, T. Wierzbicki, Protection performance of double layered metal shields against projectile impact, J. Mech. Mater. Struct. 2 (2007) 1309–1329.
[2] S. Dey, T. Børvik, X. Teng, T. Wierzbicki, O.S. Hopperstad, On the ballistic resistance of double-layered steel plates: an experimental and numerical investigation, Int. J. Solids Struct. 44 (2007) 6701–6723.
[3] P. Elek, S. Jaramaz, D. Micković, Modeling of perforation of plates and multi layered metallic targets, Int. J. Solids Struct. 42 (2005) 1209–1224.
[4] J. Radin, W. Goldsmith, Normal projectile penetration and perforation of layered targets, Int. J. Impact. Eng. 7 (1988) 229–259.
[5] X. Teng, T. Wierzbicki, M. Huang, Ballistic resistance of double-layered armor plates, Int. J. Impact. Eng. 35 (2008) 870–884.
[6] E.A. Flores-Johnson, M. Saleh, L. Edwards, Ballistic performance of multilayered metallic plates impacted by a 7.62-mm APM2 projectile, Int. J. Impact. Eng. 38 (2011) 1022–1032.
[7] G. Ben-Dor, A. Dubinsky, T. Elperin, Effect of the order of plates on the ballistic resistance of ductile layered shields perforated by nonconical impactors, J. Mech. Mater. Struct. 1 (2006) 1161–1177.
[8] M. Grujicic, B. Pandurangan, N. Coutris, A computational investigation of the multi-hit ballistic-protection performance of laminated transparent-armor systems, J. Matl. Eng. Per. 21 (2012) 837–848.
[9] P. Jantharat, R. McCuiston, C. Gamonpilas, S. Kochawattana, Influence of the laminate configurations of transparent armor on its ballistic protection, Key Eng. Matl. 608 (2014) 253–258.
[10] M. Grujicic, W.C. Bell, B. Pandurangan, Design and material selection guidelines and strategies for transparent armor systems, Matl. Design 34 (2012) 808–819.
[11] R. Klement, S. Rolc, R. Mikulikova, J. Krestan, Transparent armour materials, J. Eur. Ceram. Soc. 28 (2008) 1091–1095.
[12] K. Karthikeyan, B.P. Russell, V.S. Deshpande, N.A. Fleck, Multi-hit armour characterisation of metal-composite bi-layers, J. Mech. Matl. Struc. 7 (2012) 721–734.
[13] S. Mohan, S. Velu, Ballistic impact behaviour of unidirectional fibre reinforced composites, Int. J. Imp. Eng. 63 (2014) 164–176.
[14] O.F. Erkendirci, B.Z. Haque, Quasi-static penetration resistance behavior of glass fiber reinforced thermoplastic composites, Compos. B 43 (2012) 3391–3405.
[15] S.L. Bazhenov, G.P. Goncharuk, A study of yarn friction in aramid fabrics, Polym. Sci. Ser. A 54 (2012) 803–808.
[16] G. Gopinath, J.Q. Zheng, R.C. Batra, Effect of matrix on ballistic performance of soft body armor, Comp. Struc. 94 (2012) 2690–2696.
[17] H. Harel, G. Marom, Delamination controlled ballistic resistance of polyethylene/polyethylene composite materials, Appl. Compos. Matl. 9 (2002) 33–42.
[18] A. Levi-Sasson, I. Meshi, S. Mustacchi, I. Amarilio, D. Benes, V. Favorsky, R. Eliasy, J. Aboudi, R. Haj-Ali, Experimental determination of linear and nonlinear mechanical properties of laminated soft composite material system, Compos. B 57 (2014) 96–104.
[19] E.S. Greenhalgh, V.M. Bloodworth, L. Iannucci, D. Pope, Fractographic observations on Dyneema composites under ballistic impact, Compos. A 44 (2013) 51–62.
[20] K. Karthikeyan, B.P. Russell, Polyethylene ballistic laminates: failure mechanics and interface effect, Matl. Design 63 (2014) 115–125.
[21] P.M. Cuniff, A Design Tool for the Development of Fragmentation Protective Body ArmorProc. 18th Int. Symp. Ballistics, San Antonio, TX, Nov. 15–19 1999, pp. 1295–1302 (Dimensionless parameters for optimization of textile based body armor systems, ibid. pp. 1303–1310).
[22] K. Karthikeyan, B.P. Russell, N.A. Fleck, H.N.G. Wadley, V.S. Deshpande, The effect of shear strength on the ballistic response of laminated composite plates, Eur. J. Mech. A/Solids 42 (2013) 35–53.
[23] Z. Xue, J.W. Hutchinson, Neck development in metal/elastomer bilayers under dynamic stretchings, Int. J. Solids Struc. 45 (2008) 3769–3778.
[24] C. Chen, X. Zhu, H. Hou, L. Zhang, X. Shen, T. Tang, An experimental study on the ballistic performance of FRP-steel plates completely penetrated by a hemispherical-nosed projectile, Steel Compos. Struc. 16 (2014) 269–288.
[25] C.B. Giller, R.M. Gamache, K.J. Wahl, A.P. Saab, C.M. Roland, Coating/Substrate Interaction in Elastomer-Steel Bilayer Armor, J. Compos, Mat, 2016, http://dx.doi.org/10.1177/0021998315613131 (in press).
[26] C.W. Ong, C.W. Boey, R.S. Hixson, J.O. Sinibaldi, Advanced layered personnel armor, Int. J. Impact Eng. 38 (2011) 369–383.
[27] P. Sellappan, E. Wang, C.J.E. Santos, T. On, J. Lambros, W.M. Kriven, Wave propagation through alumina-porous alumina laminates, J. Eur. Cer. Soc. 35 (2015) 197–210.
[28] J.S. Stenzler, N.C. Goulbourne, The effect of polyacrylate microstructure on the impact response of PMMA/PC multi-laminates, Int. J. Imp. Eng. 38 (2011) 567–576.
[29] A.A. Ramadhan, A.R. Abu Talib, A.S. Mohd Rafie, R. Zahari, High velocity impact response of Kevlar-29/epoxy and 6061-T6 aluminum laminated panels, Matl. Design 43 (2013) 307–321.

[30] Y. Wang, X. Chen, R. Young, I. Kinloch, G. Wells, A numerical study of ply orientation on ballistic impact resistance of multi-ply fabric panels, Comp. B Eng. 68 (2015) 259–265.

[31] Y. Zhou, X.Z. Gong, S.Y. Zhang, A.C. Xu, A numerical investigation into the influence of layer space on panel ballistic performance, Fibers Polym. 16 (2015) 2663–2669.

[32] T. Rahimzadeh, E.M. Arruda, M.D. Thouless, Design of armor for protection against blast and impact, J. Mech. Phys. Solids 85 (2015) 98–111.

[33] C.M. Roland, D. Fragiadakis, R.M. Gamache, Elastomer–steel laminate armor, Compos. Struct. 92 (2010) 1059–1064.

[34] C.M. Roland, D. Fragiadakis, R.M. Gamache, R. Casalini, Factors influencing the ballistic impact resistance of elastomer-coated metal substrates, Philos. Mag. 93 (2013) 468–477.

[35] L. Xue, W.J. Mock, T. Belytschko, Penetration of DH-36 steel plates with and without polyurea coating, Mech. Mater. 42 (2010) 981–1003.

[36] M. Grujicic, R. Yavari, J.S. Snipes, S. Ramaswami, J. Runt, J. Tarter, G. Dillon, Molecular-level computational investigation of shock-wave mitigation capability of polyurea, J. Matl. Sci. 47 (2012) 8197–8215.

[37] A.V. Amirkhizi, J. Isaacs, J. McGee, S. Nemat-Nasser, An experimentally-based viscoelastic constitutive model for polyurea, including pressure and temperature effects, Philos. Mag. 86 (2006) 5847–5866.

[38] R.B. Bogoslovov, C.M. Roland, R.M. Gamache, Impact-induced glass transition in elastomeric coatings, Appl. Phys. Lett. 90 (2007) 221910.

[39] J.A. Pathak, J.N. Twigg, K.E. Nugent, D.L. Ho, E.K. Lin, P.H. Mott, C.G. Robertson, M.K. Vukmir, T.H. Epps, C.M. Roland, Structure evolution in a polyurea segmented block copolymer because of mechanical deformation, Macromolecules 41 (2008) 7543–7548.

[40] R. Casalini, R. Bogoslovov, S.B. Qadri, C.M. Roland, Nanofiller reinforcement of elastomeric polyurea, Polymer 53 (2012) 1282–1287.

[41] B. Arman, A.S. Reddy, G. Arya, Viscoelastic properties and shock response of coarse-grained models of multiblock versus diblock copolymers: insights into dissipative properties of polyurea, Macromolecules 45 (2012) 3247–3255.

[42] A.V. Amirkhizi, J. Isaacs, J. Mcgee, S. Nemat-Nasser, An experimentally-based viscoelastic constitutive model for polyurea, including pressure and temperature effects, Philos. Mag. 86 (2006) 5847–5866.

[43] X. Teng, T. Wierzbicki, M. Huang, Ballistic resistance of double-layered armor plates, Int. J. Impact. Eng. 35 (2008) 870–884.

[44] C.M. Roland, R.M. Gamache, Measuring the Blast and Ballistic Performance of Armor, NRL Formal Report, NRL/FR/6126-15-10,284, 2015.

[45] D.M. Hisley, J.C. Gurganus, A.W. Drysdale, Experimental methodology using digital image correlation to assess ballistic helmet blunt trauma, J. Appl. Mech. 78 (2011) 051022.

[46] B.A. Gama, S.L. Lopatnikov, J.W. Gillespie, Hopkinson bar experimental technique: a critical review, Appl. Mech. Rev. 57 (2004) 223–250.

[47] W.W. Chen, B. Song, Split Hopkinson (Kolsky) Bar: Design, Testing and Applications, Springer Science & Business Media, 2010.

[48] J. Shim, D. Mohr, Using split Hopkinson pressure bars to perform large strain compression tests on polyurea at low, intermediate and high strain rates, Int. J. Impact Eng. 36 (2009) 1116–1127.

[49] L. Brekhovskikh, Waves in Layered Media, 2nd ed.Vol. 16, Elsevier, 2012.

[50] ABAQUS, User documentation, version 6.10, Dassault Systems, 2010.

[51] C. Roland, Viscoelastic Behavior of Rubbery Materials, Oxford Univ. Press, NY, 2011.

[52] S.S. Sarva, S. Deschanel, M.C. Boyce, W. Chen, Stress–strain behavior of a polyurea and a polyurethane from low to high strain rates, Polymer 48 (2007) 2208–2213.

[53] R.L. Taylor, K.S. Pister, G.L. Goudreau, Thermomechanical analysis of viscoelastic solids, Int. J. Numer. Methods Eng. 2 (1970) 45–59.